Preparation of a diode laser for frequency stabilization to an ultra-low expansion cavity for Rydberg spectroscopy in Yb^{174}

Heinich von Stechow

Bachelorarbeit in Physik
angefertigt im Institut für Angewandte Physik

vorgelegt der
Mathematisch-Naturwissenschaftlichen Fakultät
der
Rheinischen Friedrich-Wilhelms-Universität
Bonn

July 2024

Ich versichere, dass ich diese Arbeit selbstständig verfasst und keine anderen als die angegebenen Quellen und Hilfsmittel benutzt sowie die Zitate kenntlich gemacht habe.

Bonn, 03.07.2024 ..... H. v. Stahl .....

Datum Unterschrift

1. Gutachter: Prof. Dr. Sebastian Hofferberth
2. Gutachterin: Prof. Dr. Stefan Linden

Acknowledgements

I would like to express my gratitude to Prof. Dr. Sebastian Hofferberth for the possibilty to even start my work on my thesis within his working group, the support, and encouragement throughout the course of this research. His expertise and the discussions have greatly contributed to the progress and completion of this thesis. I would also like to extend my thanks to the entire working group of the YQO experiment for providing a stimulating and collaborative environment. Especially, of course, Ludwig as my supervisor, but also the erst of the team, including Eduardo, Tangi, Xin and Florian. The experience of working with such a dedicated team has been really enriching. I have had a truly interesting time and have learned a lot.

Contents

CHAPTER 1

Introduction

The utilization of lasers in scientific endeavors has not only revolutionized our technological landscape but has also introduced scientist in profound transformations in understanding the fundamental constituents of nature. The inception of lasers in 1960, with the demonstration of the first working laser by Theodore H. Maiman, heralded a new era in the field of optics and photonics [1]. Since then, lasers have been classified into various types based on their operational principles, encompassing gas lasers, solid-state lasers, semiconductor lasers, and more recently, exotic variants such as free-electron lasers and quantum cascade lasers [2]. Each category offers unique advantages and is tailored to specific applications, ranging from industrial machining to medical diagnostics to major components in atomic physics experiments.

In the field of modern atom physics, the significance of lasers goes beyond just illumination; they serve as precise and flexible tools with long coherent times [2] for the manipulation and control of atomic systems. Central to this concept is the technique of laser cooling and trapping, which enables the confinement and manipulation of atoms at ultra cold temperatures [3]. This capability has facilitated groundbreaking discoveries in quantum mechanics and atomic physics, paving the way for advancements in fields as diverse as quantum computing, precision meteorology, and quantum simulation ([3], [4], [5]). Lasers also have the capability to excite atoms into higher energy states with remarkable precision.

Excitation of atoms is also a key component of the *Fiber Ytterbium Quantum Optics* (FYQO)-Experiment of the *Non-linear Quantum Optics* (NQO) group. The NQO group focuses on generating optical nonlinearities through light-matter interactions in various media. These interactions, in turn, affect the behavior of individual photons [6]. Specifically, the group utilizes the interactions between Rydberg excitations in an ultra-cold atomic ensemble to create effective interactions between single photons [6]. This interaction relies on the characteristics of polarizing Rydberg atoms, strong dipole-dipole-interactions and the resulting Rydberg block-

ade, which prohibits multiple Rydberg excitations on a macroscopic scale of around 1 µm [7]. Using these effects makes it possible to interact with a large amount of atoms using only one single photon, which is being used in single-photon-transistors or single-photon-absorbers [8].

The FYQO experiment aims to excite Ytterbium atoms inside a dipole trap to Rydberg states. To achieve this, Ytterbium atoms will be cooled to super low temperatures first. The cooling process consists of a 2D- and a 3D-magneto-optical-trap (MOT) which are utilized to capture the atoms such that they can be targeted by the cooling laser of the experiment. Once cooled to very low temperatures, the two-photon-excitation is practiced to excite the Ytterbium atoms in to Rydberg states. First and slightly off resonant, Yb atoms will be excited to an intermediate state, in which the atoms are not meant to stay. That is why, the atoms will be excited to an even higher state, called the Rydberg-state. Once in the Rydberg state, the interaction between Rydberg atoms will be studied.

As stated before, the laser in this experiment will be used to excite and manipulate atoms. For this, the laser has two main properties that need to be monitored closely for an effective and reproductive performance of the experiment: its natural line width and its stability in frequency over a long period of time. Commercially used *External-Cavity*-diode lasers have a natural line width of a few hundred kHz[1]. However, to cool and excite atoms, the line width of the laser should be smaller than the transition line width of the energy state targeted. With growing principal quantum number n this transition line width of Rydberg energy states decreases [10]. Therefore, to achieve Rydberg excitation, the lasers have to be held to an even narrower line width and stabilized to even less frequency drift. Hence, the success of the experiment depends on how well one manages to tackle these two challenges.
The goal of this thesis is to showcase the set-up of the laser and the optics that modify the laser beam before it enters the ultra low expansion (ULE) cavity, as well as a description of the electrical components necessary to achieve this. Although locking the laser to the cavity has not been done yet, I will briefly highlight the practical work that needs to be done to lock the laser.
To accomplish this, the thesis is structured as follows:
First, I will explore theoretical key aspects of laser technology and its applications. Initially, we will dive into the theoretical foundations of optical resonators, diode lasers, followed by a brief introduction into the Pound-Drever-Hall (PDH) laser locking technique. Further, I will show the optical set-up of the laser system, since there are two beams, in the laboratory, detailing the relevant characterization measurements like the AOM rise time and its diffraction efficiency. Finally, an outlook is given on what is left to be done on the set-up, but also to highlight their practical applications and performance within our research framework.

[1] The laser described in this work has a line width of 120 kHz, according to [9]

CHAPTER 2

Theoretical Background of diode lasers

As a result of the fundamental way in which lasers work, they produce almost monochromatic light, i.e. most emitted photons have the same frequency. One way to generate this photon emission is for excited atoms of the same element to decay into a lower energy state, whereby in this decay process a photon with the energy of the energy difference between higher and lower energy is emitted [11]. If the decay of the excited atom is caused by the hit of another photon, the newly emitted photon by the atom is emitted in the same direction as the one that flew in before. This procedure is called stimulated emission and was also utilized when the first laser in the visible spectrum was developed in 1960 [11],[1] To transit within the energy states, the atoms must absorb (when being excited into a higher energy state) or emit (when falling back to a lower energy state) photons of a specific frequency for each transition. However, fluctuations in this frequency can be evaluated over time and are called the line width of the laser. This instability in frequency has several origins, that will be discussed in the following. And since in most cases, as in this experiment, the line width of a laser is larger than transition line width of the energy state targeted in the experiment the laser must be frequency stabilized. To implement frequency stabilization, on the one hand, a very stable and narrowband reference frequency is needed. For this experiment, the reference frequency is given by an external resonator or cavity. And on the other hand, to successfully manipulate the laser frequency, a feedback loop consisting of different electronic components needs to be implemented (see section 2.3 for more details). This feedback loop then adjusts the laser frequency by typically changing the laser diode current and the piezo transducer [12]. This ensures the laser remains closely aligned at the desired frequency, based on the detected deviations.

2.1 Optical resonators

If not stated differently, the following details about the theoretical background in this section are taken from [13].
In the most general form, optical resonators consist of two parallel mirrors, that capture electromagnetic waves. In their application in lasers, one of the mirrors is typically fully reflective whereas the other is only partially reflective with reflectivity R. This means, there is a fraction of the wave with intensity I that gets reflected, i.e. $R \cdot I$, while the remaining part of the wave is transmitted. Hereby, resonators act as *mode selectors*, i.e. only reflecting those modes that are resonant to the resonator length.
A wave of frequency ω is described by [2]

$$E(r,t) = \mathfrak{Re}\left[E_0(r)e^{(i\omega t)}\right], \tag{2.1}$$

where E_0 is the amplitude of the wave and $\omega = c_n k$. In the case of two plane-parallel mirrors and without losses, the tangential component of the em wave must vanish at the mirrors, i.e. $E(\mathbf{r}) = 0$ at both mirrors, giving us boundary conditions at $z = 0$ and $z = L$. With this, the solution of the Helmholtz-equation,

$$\nabla^2 E(r) + k^2 E(r) = 0\,, \tag{2.2}$$

is given by a standing wave [2]:

$$E = E_0 \sin(kz) \tag{2.3}$$

Using the given boundary conditions, one finds for k, the wave vector, a discrete distribution

$$k_n = \frac{n\pi}{L}, \text{ with } n \in \mathbb{N} \tag{2.4}$$

Except for $n = 0$, which leads to $\sin(0 \cdot z) = 0$ which is not a physical solution and thus neglected, eq. 2.4 results in an infinite number of possible modes [2]. The resulting em field inside the resonator can be described as superposition of stationary waves:

$$E(r) = \sum_n E_n \sin(k_n z) \tag{2.5}$$

Just as k_n, the frequency ω of the wave, due to its dependency on k_n and the constant c, only takes on discrete values as well.

Another important property of an optical resonator is its *free spectral range*. It depends on the refractive index n of the material inside of it and the length L of the cavity, which can be seen in fig. 2.1(a). As mentioned before, certain frequencies will be transmitted more

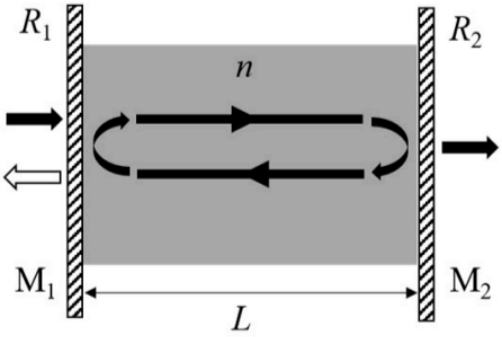

(a) Sketch of a resonator consisting of parallel mirrors M_1 and M_2 with reflectivities of R_1 and R_2, respectively, surrounding a cavity medium of refractive index n and thickness L [14]

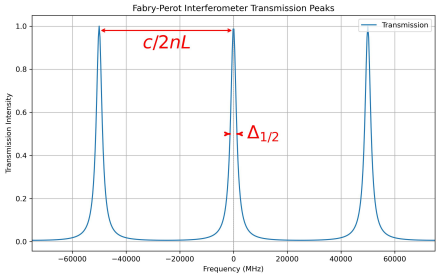

(b) Transmission of a planar opt. resonator showing frequency spacing (i.e. the FSR) of adjacent longitudinal modes and the full-width at half-maximum ($\Delta_{1/2}$). Here $n = 3$, $L = 1$ mm and $R = 0.98$

by a resonator than others. This is because only modes resonant to twice the length of the cavity resonate with it and get reflected. The free spectral range is the difference between two frequencies, at which the transmission of light is at a maximum, see fig 2.1(b).

$$\Delta\nu_{\text{fsr}} = c/2nL \tag{2.6}$$

If one would assume a resonator length of approx. 1 mm and a refractive index $n = 2$, this results in a free spectral range in the order of magnitude of 10^{10} Hz or GHz.
Resonators provide narrow spectral reference frequencies characterized by sharp resonance peaks [15]. The physical background to this can be illustrated using the example of the *Fabry-Perot* interferometer.
Similar to the previously described resonators, Fabry-Perot interferometers consist of two plane and parallel mirrors, which act as frequency filters. How good of a frequency filter the Fabry-Perot interferometer is, is reflected by the *Finesse*, $\mathcal{F}$:

$$\mathcal{F} = \frac{\Delta\nu_{fsr}}{\Delta\nu_{1/2}} = \frac{\pi\sqrt{R}}{1-R}\,. \tag{2.7}$$

Here, $\Delta\nu_{fsr}$ is the free spectral range, described in eq. 2.6 and $\Delta\nu_{1/2}$ is the full-width-half-maximum (FWHM) of the resonance peak. In order to lock a laser with a very narrow line width to an external cavity, one needs a cavity with a high finesse [16].
In reality, the mirrors of the resonator are not perfect reflectors, i.e. there are always photons that get absorbed by or pass through the mirror, which causes the photons to leave the resonator. If you assign a specific loss-factor β_k to each mode k, the energy W_k stored in the

mode decreases exponentially over time:

$$W_{\mathrm{k}}(t) = W_{\mathrm{k}}(0)e^{-\beta_{\mathrm{k}}t} \tag{2.8}$$

This leads to an average residence time in the resonator of $\tau = 1/\beta_{\mathrm{k}}$. Since the energy of the beam is proportional to the intensity I of it, one gets the same exponential decay of the intensity depending on the loss factor. With this, the finesse can be reinterpreted as residence time of the photons in the resonator.

To quantitatively describe the behavior of the reflected beam, we select a point outside the cavity and measure the electric field over time. The magnitude of the incident beam's electric field can be expressed as $E_{\mathrm{in}} = E_0 e^{i\omega t}$, whereas the electric field of the reflected beam is described by $E_{\mathrm{ref}} = E_1 e^{i\omega t}$ [15]. Note, that the amplitudes of both electric fields are complex in order to reflect the relative phase difference between both fields. The reflection coefficient $F(\omega)$ represents the ratio of E_{ref} to E_{in}. For a symmetric cavity without losses, it is defined as [15]:

$$F(\omega) = \frac{E_{\mathrm{ref}}}{E_{\mathrm{in}}} = \frac{\sqrt{R}\left(e^{i\omega/\Delta\nu_{\mathrm{fsr}}} - 1\right)}{1 - \mathrm{R}e^{i\omega/\Delta\nu_{\mathrm{fsr}}}} \tag{2.9}$$

The intensity of the beam is then calculated by [15]:

$$\begin{aligned} I_{\mathrm{ref}} &= \left|FE_{\mathrm{in}}\right|^2 \\ &= I_0 \frac{\sin^2\left(\frac{\omega}{2\Delta\nu_{\mathrm{fsr}}}\right)}{(\pi/2\mathcal{F})^2 + \sin^2\left(\frac{\omega}{2\Delta\nu_{\mathrm{fsr}}}\right)} \end{aligned} \tag{2.10}$$

The reflected beam is later measured on a photodiode to detect the difference between actual and wanted laser frequency, more of it in section 2.3.

2.2 Laser principles

2.2.1 General assembly of a laser

A laser has three main components: the energy pump, the active medium, and the resonator. The energy pump supplies the necessary energy to the atoms of the active medium, typically through electrical current or light with sufficient intensity to push them into excited energy states. When these excited atoms decay to lower energy states, they emit photons. It is

called *active medium* because population inversion is created in it [2]. Population inversion in a medium occurs when more atoms are in an excited state than in the ground state. Hence, the electrical current or the pumping light ensures that population inversion exists, creating the condition necessary for stimulated emission [2]. The intensity of the light or the current at which population inversion is achieved and maintained, is called the threshold condition I_{thr}. However, with only two energy states, i.e. the ground and the excited state, population inversion cannot be maintained. This is because if there are the same number of atoms in the ground and excited states, absorption and stimulated emission processes will compensate each other [2]. This results in the fact, that stimulated emission is no longer the dominant process. However, this is necessary for the generation of the laser beam. Therefore, the atoms must be excited into states from which they do not decay directly back in to the ground state, but first via one or two intermediate states. These are then referred to as *three-* or *four-level lasers* [2]. To initiate population inversion, the pumping mechanism have to obtain the threshold condition. Here, the oscillation and amplification of photons inside the resonator will start when the gain of photons from the active material compensates the losses inside the lasers (e.g. losses due to the outgoing beam)[2].

The resonator of the laser, which necessarily do not have to consist of two mirrors, reflects the emitted photons inside of it. This configuration ensures that the emitted photons once reflected by the resonator stimulate further emissions in the active medium, creating a cascade of photons that are highly coherent and monochromatic. With this, amplification and single mode selection, as mentioned in sec. 2.1, is achieved, which is the essence of laser operation. First, the resonator selects only very few modes that get reflected inside the resonator, depending on its free spectral range. Secondly, one mode will dominate the amplification process stimulating more emission of photons of the same frequency than the other modes. The resonator just referred to should not be confused with the external resonator described in the introduction to this chapter and more detailed in sec. 2.3. The resonator built into the laser is an essential component of it, designed to amplify the light and select a single mode to be emitted. Whereas, the external resonator, an *Ultra-Low-Expansion*-cavity, serves as a reference frequency in order to determine whether the frequency of the emitted laser light still matches the needed frequency.

2.2.2 Working principle

The laser used in this experimental set-up and described in the following is a semiconductor or diode laser. What is special about diode lasers is that they consist of a crystal, that is separated in to two layers, p and n-layers, with each layer being doped with a different semiconductor material [2]. Bringing these two layers together forms a pn-junction. In

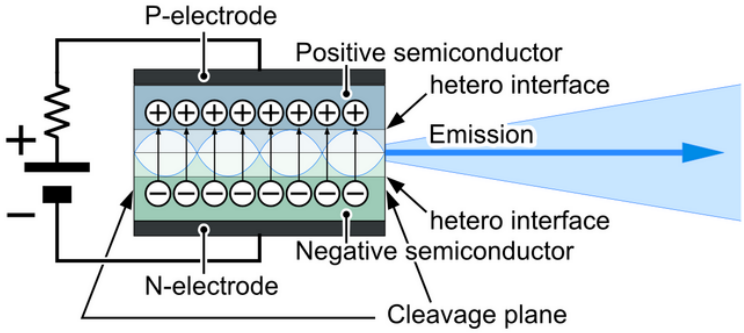

Figure 2.2: Internal structure of a diode laser, taken from [17]

the narrow area around this junction and without further electrical fields applied, negative charges recombined with positive holes, yielding in a neutral area inside the diode, as seen in fig. 2.2 as the area between the negative and the positive semiconductor. Applying voltage to the diode leads to even more recombination of electrons and holes, because the resulting electrical field pulls even more electrons towards the positive holes and vic versa [2]. This increases the neutral area. To understand the recombination of free electrons with positive holes and how in this process photons are emitted, one needs to understand the concept of *bands* [18]. The free electrons are considered to be in the conduction band, i.e. they move around the crystal freely. When these free electrons recombine with holes again, the positive core of the hole attracts the electron so strongly that it can overcome the band gap between the conduction band and the valence band. The energy overcome from the conduction band to the valence band is released in the form of a photon with the same energy. Therefore, the light emitted from this recombination process is also characteristic of each semiconductor, since they differ in their band gaps [2] It also depends on the doping [13]. If the threshold current I_{th} is reached, there is more recombination and therefore spontaneous emission of light. The emitted photons get reflected inside the semiconductor crystal, create stimulated emission and lead to a strong em field in the form of a strongly coherent laser beam. The „cleavage planes“, as it is called in figure 2.2, act as the mirrors of the resonator.
Another way of keeping the line width of a laser stable and sufficiently narrow for the experiment, is to decrease naturally occurring thermal, electric and acoustic noise. For example, heating or cooling the diode crystal to keep its temperature stable. Inside the laser housing, the so-called *Littrow*-configuration is implemented. This configuration functions as another resonator using the far side of the crystal's „cleavage plane“, the left one in fig. 2.2, and uses a diffraction grating as the other cavity mirror. If the grating is at a certain angle to the incident beam, since optical gratings produce an interference pattern, one of the created

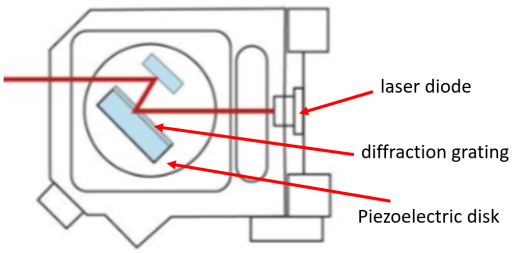

Figure 2.3: Internal set-up of an ECDL [20]

maxima can be reflected into the laser diode [2]. In our case, it's the first-order diffraction from the grating that is coupled back into the laser diode, while the directly reflected light, i.e. the „0^{th} order", forms the output beam. The beam that is reflected into the laser functions as a feedback signal for the laser, because it causes more stimulated emission of the same frequency in the active medium. A piezoelectric transducer disk under the grating is used to modify its angle to the beam, which is equivalent to changing the cavity length, and by doing so, the resonance of the cavity [19]. This can therefore also be used to tune the wavelength [2]. A scheme of the set-up of the diode laser can be seen in figure 2.3.

2.2.3 Laser modes

An optical resonator determines both the frequency and spatial distribution of light. The wavefronts of the modes within the resonator must match the mirror curvatures. This is, because the focal point of the curved, non-transmitting mirror must be on the partly transmitting mirror. Only then one obtains low-order transverse modes The simplest mode is a Gaussian beam, whose electric field $E(r,z)$ at a radial distance r from the centre axis and axial distance z from the beam focus is [2]:

$$E(r,z) = A\frac{w_0}{w(z)}\exp\left(-\frac{r^2}{w^2(z)}\right)\exp\left(-i\left(kz+\frac{kr^2}{2R(z)}-\zeta(z)\right)\right) \tag{2.11}$$

where w_0 is the beam waist, $w(z)$ the Beam radius at distance z, $R(z)$ the radius of curvature of the wavefront and $\zeta(z)$ is the Gouy phase. The intensity $I(r,z)$, proportional to the square of the electric field $|E|^2$, is:

$$I(r,z) = I_0\left(\frac{w_0}{w(z)}\right)^2\exp\left(-2\frac{r^2}{w^2(z)}\right) \tag{2.12}$$

The Gouy phase $\zeta(z)$ is defined by:

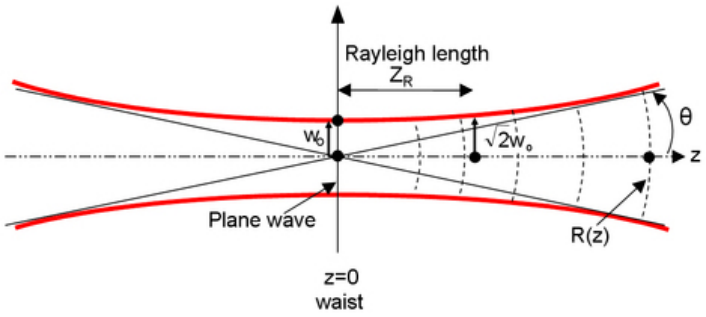

Figure 2.4: A Gaussian beam with its characteristic measures [21]

$$\zeta(z) = \arctan\left(\frac{z}{z_0}\right) \tag{2.13}$$

Beyond the fundamental Gaussian mode, higher-order modes are described by Hermite-Gaussian beams, which have more complex intensity distributions, see [22] for more information on that. Here, only the resonance frequencies for these modes, both, fundamental and higher-order, are of interest, with transverse mode indices m and n:

$$\nu_{q,m,n} = q\Delta\nu_{\mathrm{FSR}} + (m+n+1)\,\frac{\Delta\zeta}{\pi}\Delta\nu_{\mathrm{FSR}} \tag{2.14}$$

with $\Delta\zeta$ being the difference in Gouy phase [13].
Modes with different longitudinal indices q but the same transverse indices display the same intensity distribution and are described as TEM_{mn} (transverse electric and magnetic) modes. For certain Gouy phase shifts (e.g., $\pi, \pi/2, \pi/4$), mode *frequency degeneracy* can occur, leading to overlapping modes and potential deterioration of the coherence of the beam. To avoid frequency degeneracy and ensure high-quality beam output, proper resonator design is crucial. For example, a resonator with a length of $L = 100.1$ mm, mirror curvature of $r_2 = 500$ mm and $r_1 \to \infty$ can achieve a transverse mode frequency spacing of 221 MHz, minimizing degeneracy and allowing the fundamental Gaussian mode to serve as a reference frequency for laser stabilization.

2.3 Pound-Drever-Hall (PDH) Laser Stabilization

Methods such as changing the voltage applied to the piezo to adjust the orientation of the grating to the beam, which is used for wave length tuning, are already used within the laser housing to narrow down the line width of the laser. Since these methods only narrow down

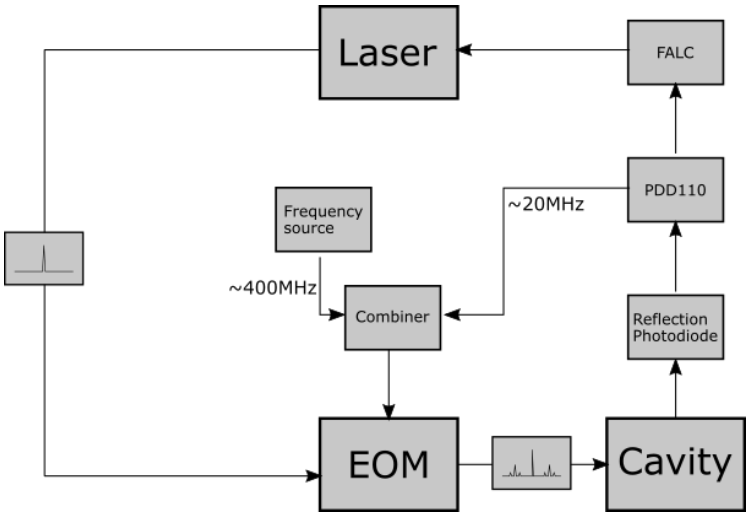

Figure 2.5: The electronic configuration for PDH locking involves modulating the carrier frequency with sidebands. The reflected signal from the cavity is then detected by a photodiode and further processed using a phase shifter (PDD110), a mixer, and a low-pass filter (inside FALC). The combiner acts as a power splitter. This processed signal, which represents the error signal, is subsequently used to adjust the laser.

the line width without reducing the frequency drift, scientist developed a new method of frequency stabilizing. This method is called *Pound–Drever–Hall* frequency stabilization and uses an external resonator to lock the laser frequency to the external reference frequency. The technique has been used to demonstrate, using a commercial laser, a frequency standard as relatively stable as a pulsar [15]. In the following, I will go over the key theoretical aspects needed to accomplish successful frequency stabilization.

Note: The information in the following section about the theoretical background of the PDH-technique are, if not stated differently, all gathered from E. D. Black's paper „An introduction to Pound–Drever–Hall laser frequency stabilization ", [15]

The concept underlying the Pound-Drever-Hall technique is straightforward: it involves evaluating a laser's frequency using an optical resonator, with this evaluation being relayed back to the laser to mitigate frequency instabilities. This process is achieved through a type of lock-in detection, which effectively separates the frequency measurement from the laser's output intensity.
To be more precise, evaluating the laser frequency means that an error signal is generated. This signal will then result in a feedback signal to correct frequency instabilities . The error

signal can theoretically be derived from both the reflected and transmitted light signals, leveraging the optical characteristics of the resonator. Since the laser operates near the cavity's resonance frequency, it is challenging to distinguish between intensity and frequency fluctuations, which both have an effect on the transmitted intensity, see fig. 2.1(b). The reflected signal provides a frequency-dependent output that is symmetric around the resonance point. However, this does not provide information on the direction of frequency deviations. The phase of the reflected signal, which is antisymmetric around the resonance, is crucial for determining whether the frequency is above or below the resonance. This phase information can be obtained from the derivative of the reflection coefficient. Once a measure of how the reflected intensity changes with respect to frequency is obtained, this information can be used to adjust the laser, ensuring it remains aligned with the cavity's resonance frequency. Precisely, The core objective of the Pound–Drever–Hall technique is this stabilization. To achieve this, it is necessary to modulate the laser light with sidebands. The sidebands can be generated via phase modulation of the laser light, e.g. with an *electro-optic-modulator* (EOM). An Electro-Optic Modulator (EOM) functions similarly to an adaptive wave plate, as it is a crystal that swiftly alters its refractive index in response to electrical signals. This induces a slight phase shift in the passing light. The modulation frequency should be significantly higher than the cavity's line width to ensure that the sidebands are fully reflected when the carrier frequency is near the cavity's resonance. Subsequently, the reflected signal from the cavity mirrors is detected by a photodiode and further processed with a phase shifter, mixer, and low-pass filter. While the phase shifter corrects the delay that the two rays have with respect to each other, the mixer works like a multiplier of the two inputs, one is the modulation frequency by the RF-generator and another signal. Subsequently, a low-pass filter suppresses frequencies oscillating faster than Ω, generating a clean error signal. The resulting error signal is then fed back into the laser via a PID controller to maintain the laser's frequency lock at the cavity's resonance. The schematic diagram of the set-up for generating the error signal is illustrated in Fig. 2.5. The underlying principles are mathematically described in the following sections, with detailed derivations available in [15].
The following section is dedicated to the mathematical description of the phase modulation. Once the beam has traversed the EOM, its electric field undergoes phase modulation, resulting in a laser beam with frequency ω and sidebands of amplitude β and modulation frequency Ω:

$$E_{\text{inc}} = E_0 e^{i(\omega t + \beta sin\Omega t)} \tag{2.15}$$

Rewriting this expression using the Bessel functions [23] yields in:

$$\begin{aligned} E_{\text{in}} &= E_0 e^{i\omega t} \sum_{-\infty}^{\infty} J_n(\beta) e^{in\Omega t} \\ &\approx E_0 \left[J_0(\beta) e^{i\omega t} + J_1(\beta) e^{i(\omega+\Omega)t} - J_1(\beta) e^{i(\omega-\Omega)t} \right] \end{aligned} \tag{2.16}$$

Because of the sidebands, there are actually three distinct beams incident on the cavity: a carrier beam with angular frequency ω, and two sidebands with frequencies $\omega \pm \Omega$, where Ω denotes the phase modulation frequency and β represents the modulation depth. Assuming that the total power in the incident beam is $P_0 = E_0^2$, the power in the carrier beam is:

$$P_c = J_0^2(\beta) P_0, \tag{2.17}$$

where $J_0(\beta)$ is the zeroth-order Bessel function of the first kind evaluated at β.
The power in each first-order sideband is given by:

$$P_s = J_1^2(\beta) P_0, \tag{2.18}$$

where $J_1(\beta)$ is the first-order Bessel function evaluated at β.
For small modulation depths ($\beta \ll 1$), almost all the power is concentrated in the carrier and the first-order sidebands, such that:

$$P_c + 2P_s \approx P_0. \tag{2.19}$$

The wave function of the reflected beam is then described by:

$$E_{\text{ref}} = E_0 \left[F(\omega) J_0(\beta) e^{i\omega t} + F(\omega+\Omega) J_1(\beta) e^{i(\omega+\Omega)t} + F(\omega-\Omega) J_1(\beta) e^{i(\omega-\Omega)t} \right]. \tag{2.20}$$

Finally, the power of this superposition of beams is measured on a photodiode. This produces both constant terms and, at multiples of ω, oscillating terms. This gives us: With $P_{\text{ref}} = \left| E_{\text{ref}} \right|^2$, this gives us:

$$\begin{aligned} P_{\text{ref}} = P_{\text{c}} |F(\omega)|^2 &+ \left| P_s \{ |\ F(\omega+\Omega) \right|^2 + |F(\omega-\Omega)|^2 \\ &+ 2\sqrt{P_c P_s} \{ \mathfrak{Re}[F(\omega) F^*(\omega+\Omega) \\ &- F^*(\omega) F(\omega-\Omega)] \cos\Omega t + \mathfrak{Im}[F(\omega) F^*(\omega+\Omega) \\ &- F^*(\omega) F(\omega-\Omega)] \sin\Omega t \} + (2\Omega \text{ terms}) \end{aligned} \tag{2.21}$$

The error signal ϵ is defined as follows:

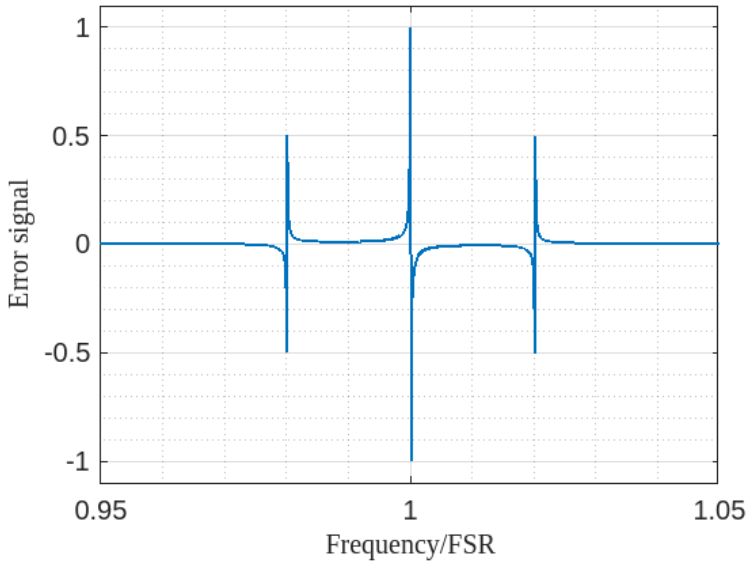

Figure 2.6: PDH error signal

$$\epsilon = -2\sqrt{P_c P_s} \cdot \Im\mathfrak{m}[F(\omega)F^*(\omega+\Omega) - F^*(\omega)F(\omega-\Omega)] \tag{2.22}$$

The calculated error signal is shown in fig. 2.6. In the case of resonance, performing a scan in proximity to the resonance yields a linear response characterized by the following equation:

$$\epsilon \approx D \cdot \delta f \qquad \text{mit} \quad D = -\frac{8\sqrt{P_c P_s}}{\delta\nu} \tag{2.23}$$

This signal can be fed back to the laser to adjust and stabilize both the carrier and the sideband frequencies. Figure 2.6 show the course of an PDH error signal of a cavity with a free spectral range $FSR = 1.497\,\text{GHz}$, a reflectivity coefficient $R = 0.9998$[1] and a modulation frequency of $\nu_{\text{mod}} = 30\,\text{MHz}$.

[1] The actual reflectivity of the mirrors in the cavity of this experiment depends on the incident wavelength. For 795 nm the reflectivity coefficient will be between $R = 0.99992561$ and $R = 0.99991649$ [24]. The reason why a reflection coefficient of 0.9998 was chosen is that it makes the course of the error signal of the PDH method easier to identify.

CHAPTER 3

Structure of the laser system

In the preceding chapter, the theoretical principles governing laser operation were covered. This chapter will now shift focus to the technical specifications of the laser and its integration into our experimental set-up. This experiment uses a diode laser by *TOPTICA Photonics AG* called *TA-SHG pro*. This laser outputs two beams: one with an infrared and one with a blue wavelength.
The following chapter will go over the experiment's laser system and describe the used optical components in the beam path of the infrared and the blue beam. It will outline the characteristics of the different optics and their importance for the experiment. Not only the optical, but also the electronic components of the set-up are explained and their operating principle is described.
The infrared beam is directed through various optical components into the *ultra-low-expansion* (ULE) cavity. Simultaneously, a split part of the beam is sent to a wavemeter to continuously monitor the laser frequency. The different optical components used to modulate the beam, such as acousto- or electronic-optical modulators, will be described in more detail in the following.
The blue beam is created by frequency doubling the infrared beam and is therefore inherently linked to the latter. This dependency ensures that changes in the infrared beam, e.g. from frequency modulation, are mirrored in the blue beam. The blue beam will later be used in the main experiment to excite the atoms in a dipole trap from the intermediate state into the Rydberg state.

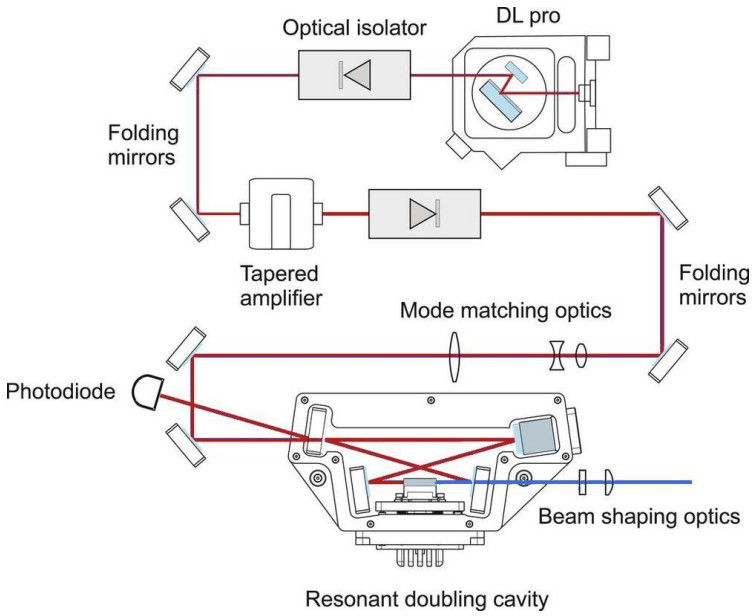

Figure 3.1: scheme of the internal set-up of the laser, outlining the beam path, the TA, bow-tie-configuration and the blue output beam, from [27]

3.1 Operational mode of the laser

The *TA-SHG pro* laser is a tunable external cavity diode laser (ECDL). Its way of working was described in sec. 2.2. What comes out of the laser housing as infrared beam is actually leakage that penetrates the first mirror in the laser. This beam outputs 790 nm with a measured intensity of (2.21 ± 0.01) mW [1]. A more detailed view of the internal set-up of the laser can be seen in fig. 3.1 and the appendix of this work. Inside the housing of the laser, the reflected infrared beam then passes the *tapered amplifier*, or *TA* for short, where the beam is amplified. The beam is then guided into a *bow-tie*-cavity, seen in the lower half of fig. 3.1, in which *second-harmonic-generation*, or *SHG*, unfolds. *SHG* describes the process of frequency-doubling the incoming light. Here, frequency doubling is realized by a non-linear crystal. For more details on second-harmonic-generation and frequency doubling, see [25] and [26]. Simplified, two incident 790 nm photons combine in th non-linaer crystal to create a single 395 nm photon of double frequency.

[1] All the following intensity measurements were taking with the power meter PM100D and the appropriate photodiode of the C-Series, both manuactured by *Thorlabs*

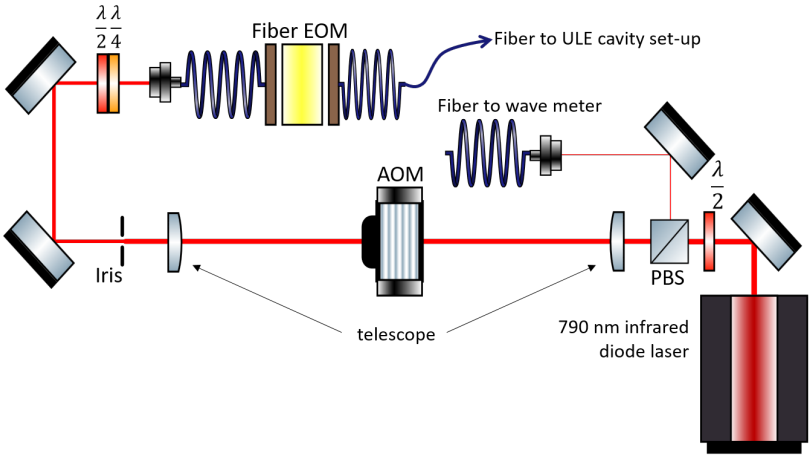

Figure 3.2: symbolic set-up of the used optical components in the infrared beam

3.2 Infrared laser beam

3.2.1 Set-up of the optical components

The set-up of the optical components is shown in fig. 3.2. The first $\lambda/2$- wave plate, as it can be rotated manually, serves to regulate the intensity of the beam. That is because it rotates the polarization of the beam, leading to either more or less transmission of horizontally polarized light at the following *polarizing beam splitter*. The PBS, for short, then splits the incident beam. Depending on the orientation of the polarization, parts of the light get transmitted, while the remaining part is reflected on the diagonal plane inside the cube. The reflected beam, guided by a mirror and damped by an ND filter[2] with an optical density of 2.0[3], then enters a multimode fiber, which leads to a wavemeter[4]. This ensures the constant measurement and evaluation of the beam frequency. Evaluating the laser frequency is important to check whether the PDH method achieves the desired results. The frequency measured[5] using the wavemeter, which has a nominal accuracy of 600 MHz showed (379.7407 ± 0.0006) THz, which equals to a wavelength of (789.466 ± 0.001) nm. The transmitted beam at the PBS enters a telescope consisting of two convex lenses with their curved surfaced pointing towards each other. Both lenses have their focal point at $f = 150$ mm. In the focal point of the

[2] NE20A by *Thorlabs*

[3] Optical density (OD) indicates the attenuation factor provided by an optical filter, i.e. how much it reduces the optical power of an incident beam [28]

[4] Model Wavelength Meter Ångstrom WS/6-200 by *High Finesse*

[5] This measurement was taken with no further stabilization methods applied

telescope, an AOM is placed. The AOM diffracts the beam into several intensity maxima. Here we are interested in the first intensity maximum to the left, i.e. the -1^{st}-order. For a more detailed description of this process, see sec. 3.2.2. To isolate this maximum from the rest of the interference pattern, an iris is placed behind the telescope.

3.2.2 Acousto-optical modulator in the infrared beam

The key element of an AOM is a transparent crystal (or piece of glass) through which the light propagates and a transducer attached to it used to excite a sound wave.
The input RF-signal of the AOM creates an oscillating mechanical pressure of a sound wave. When an acoustic wave propagates through an optically transparent medium, such as a crystal in our case, it induces a periodic modulation in the refractive index via the acousto-optic effect [29]. The modulation of the carrier frequency of the laser beam is given by the modulation frequency applied to the AOM [30]. In this case, the modulation frequency is equal to the center frequency of the AOM. At this center frequency, the Bragg condition inside the crystal is met [31]. In general the modulation frequency does not have to be equal to the center frequency though. This modulation creates an interference pattern that diffracts portions of incident light into interference maxima. A device that generates this type of diffraction by transmitting radio frequency (RF) pulses onto its transparent medium is known as an acousto-optic modulator [29].
Here, a model from Crystal Technologies[6] is used. The input RF signal of the AOM in the infrared beam is at 80 MHz. Since the following iris isolates the targeted order from the light in the other orders and only the -1^{st}-order is coupled into the fiber, the AOM can be used to switch the beam on and off very quickly. Without RF-signal, the beam does not get diffracted in the AOM and it would be dumped on the iris. This is very important when used in the blue beam, in order to only irradiate the trapped atoms for a certain time. That is, because as soon as the atoms are in the excited state, i.e. the Rydberg state, and they were to be illuminated further, they would be stimulated to fall back to the ground state, which is not the intended outcome. Looking at thr light in the -1^{st}-order means that the frequency of the laser beam was shifted down by 80 MHz. The 1^{st}-order would result in an uplift of the laser frequency by the amount of the modulation frequency.
How quickly the beam can be turned on and off, is given by its rise time. To measure its rise time, one output channel of a function generator is connected to the AOM. The same channel of the frequency generator is also connected to an oscilloscope. Behind the iris, a photodiode [7] is placed to measure the beam coming out of the AOM. The photodiode needs to have a very short reaction time, so that it can register and forward incoming signals in a

[6] Model number: 3080-122
[7] DET36A2 by *Thorlabs*

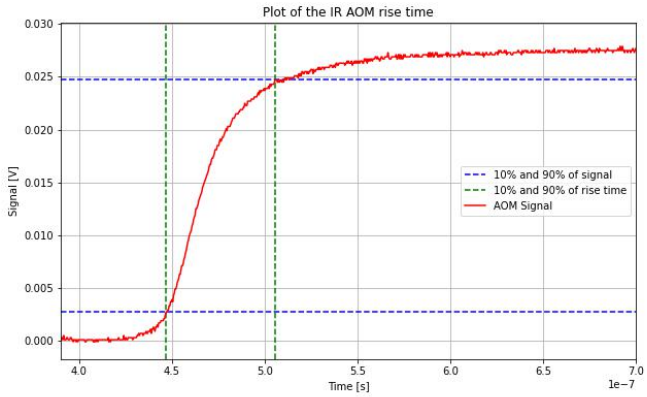

Figure 3.3: Plotted data from the oscilloscope with dotted lines marking the moment the photodiode signal and therefore the beam reaches 10% and 90% of the full amplitude

very short time. This is crucial if the temporal progression of a light signal is to be detected, like in the case of measuring the rise time of an AOM. The photodiode is also connected to the oscilloscope, but on a different channel. In this way, both signals can be seen next to each. The signal that the photodiode detects shows an error-function-like course and can be seen in the appendix. The time it takes for the photodiode signal, i.e. the laser beam, to go from 10% to 90% of its amplitude, is called the rise time and was calculated using the data from the oscilloscope. This resulted in a rise time of 58.8 ns. Because the oscilloscope does not show any errors and the Photodiodes noise is negligibly small, error calculations for the rise times were omitted here. Additionally, using the `Gaussian Beam` software, a program that simulates beam paths, as a theoretical reference point, a beam diameter of 89.3 µm was calculated. The manufacturer does not provide a rise time for a beam diameter of below 200 µm, see [32]. According to the spec sheet of this AOM the rise time for a 830 nm beam of 200 µm diameter is 34 ns. Since the rise time increases for larger beam diameters, this contradicts the measured value. There are several reasons for this. Firstly, it is conceivable that the Gaussian beam is not exactly waisted in the center of the AOM. Perhaps the beam diameter is not yet at its narrowest point or is already spreading out again. In both cases, this results in a longer rise time because the sound wave needs more time to pass through a larger beam. Another reason for the result deviating from expectations could be the electronic components within the AOM. This is supported by figure 3.3, where one can see a flattening curve of the photodiode signal well before the 90% mark is reached. A delay in the processing of the RF-Signal could therefore also have its roots in the electronic circuit of the used AOM. Since the photodiode was also used to measure the rise time of the AOM in the blue beam

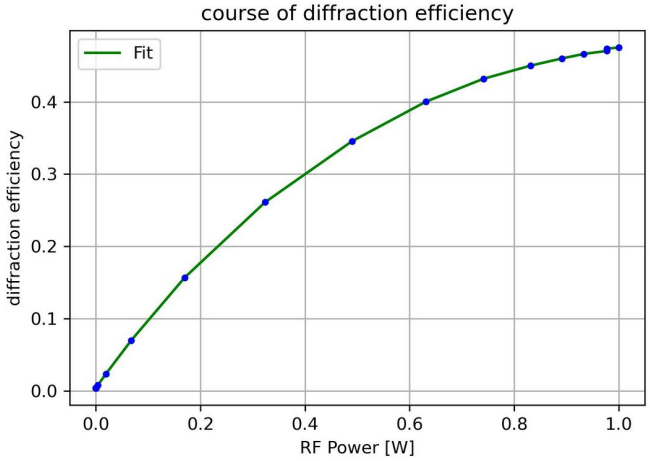

Figure 3.4: Diffraction efficiency of the AOM in the infrared beam. For this, the ratio of measured intensity in the first order and the intensity before the AOM was determined each time

(see sec. 3.3.2) without showing the same result or error, it can be ruled out as a source of error. In summary, the measured result does not exactly match expectations, but the reference value and measurement result are within a range that can be explained by the errors listed.

Furthermore, it was measured how the intensity of the beam before compares to the one right after the AOM, as well as how the diffraction efficiency depends on the input RF power. The first measurement confirms the maximum of 3% insertion loss [32], which is given in the specs, because the beam in front of the AOM measured an intensity of $(2.13 \pm 0.02)\,\mathrm{mW}$ and right after it $(2.09 \pm 0.02)\,\mathrm{mW}$. This equals almost 2%. The diffraction efficiency is calculated by looking at the intensity of the beam in front of the AOM and after the AOM in the first order. The result is shown in figure 3.4. The efficiency reached with this set-up in the -1^{st} order is 47%. This means that the beam after the AOM and when it hits the fiber coupler, has an intensity of just over $(1.005 \pm 0.001)\,\mathrm{mW}$. There, a coupling efficiency into the fiber of 31% is realized. Normally, significantly higher efficiencies can be achieved here. Nevertheless, $300\,\mu\mathrm{W}$ is adequate for the subsequent application of the beam for frequency stabilization in the ULE configuration. The used fiber here is a *single-mode* fiber, that maintains the polarization of the beam[8]. Part of this fiber is the fiberEOM.

[8] phase modulator, $LiNbO_3$, model no. PM785 by *Jenoptik*

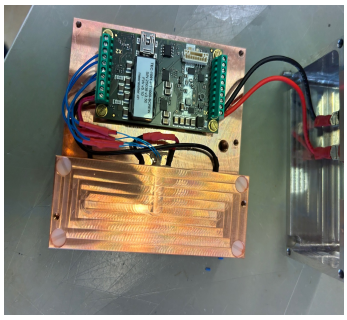

(a) Temperature controller, *TEC 1091* by *Meerstetter*, of the EOM

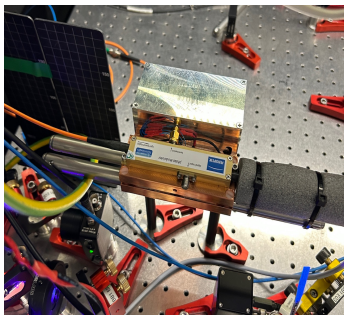

(b) Exp. Implementation incl. isolated fiber for temperature stabilization

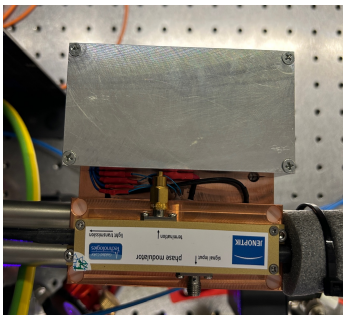

(c) optical In- and Output and electrical signal input of the EOM

3.2.3 fiber electro-optical modulators

Conceptually, electro-optical modulators (EOM) work according to the same principle as the AOMs just described. The difference between these two modulators is that in EOMs an electric field induces a change in the refractive index of a material, thereby modulating the optical signal passing through it. This modulation can be achieved by fast changes of the electrical signal, making EOMs suitable for applications requiring quick and accurate control of light [33].
In this experiment, the EOM is used to modulate sidebands to the carrier beam for the PDH locking, as well as tuning the laser frequency to lock it to the ULE. Figure 3.5(a) - 3.5(c) shows the internal set-up of the temperature control system (left) and its implementation in the experimental set-up (middle, right).
In order to modulate the sidebands on the carrier, the EOM gets an input signal from an RF-source. In the modulation process, the RF signal from the *SynthUSB II*, see sec. 3.2.4 for more details on this, drives the EOM crystal to create periodic changes of its refractive index. These changes effectively impose the RF signal onto the optical beam, creating sidebands around the carrier frequency. The sidebands are essentially additional frequency components that are symmetrically spaced apart from the carrier frequency by an amount equal to the frequency of the modulation signal. Later, they are important to lock a laser to the cavity at a specific frequency.

3.2.4 Frequency stabilization using USB RF Signal Generator

The *SynthUSBII* manufactured by *Windfreak Technologies*[9], is a compact RF signal generator that operates over a frequency range from 35 MHz to 4.4 GHz [34]. One of the key features

[9] Link to the product website

of this RF generator is that it is powered and controlled via USB, which simplifies the set-up and operation of the device. The control software provided by the manufacturer allows for adjustment of the output frequency, output power, and other parameters.
Because of the frequency modulated on the beam in the crystal of the EOM, the phase of the beam is changed, as seen in sec. 2.3. For this laser a frequency modulation of 15 MHz is being used.
The set-up of the used electronics for this can be seen in fig. A.3 in the appendix. The housing consists of a USB-Hub, that can take in four different RF-signal generators and establishes the USB connection to the computer. Each channel then has a *Minicircuits ZFSC-2-2500-S+* power splitter to combine the main sideband frequency (Windfreak RF-generator) and the PDH sideband frequency (via Toptica PDD-110). In fig. 2.5 this is called „Combiner“. The error output of the PDD110 is also fed to the FALC (fast analog line width control), which is a module for advanced laser frequency stabilization, i.e. decreasing line width and high-bandwidth frequency locking. The FALC contains a PID which then eventually impose a change in the electronic discharge of the diode. The amplification is done by *Minicircuits ZFL-1000VH+* power amplifier, providing 22 dB amplification at up to 1 GHz. The combination of the signals is then applied back on to the EOM. After the EOM, the infrared light gets to the optical set-up in front of the ULE cavity.

3.2.5 Ultra Low Expansion Cavity

The infrared beam at 795 nm will be the fourth laser locked to the ULE cavity. This is the maximum number possible for this cavity. A 3D model of the planned set-up, that would make it possible to lock a fourth laser to the cavity, is pictured in fig. 3.6. Another picture of the optical components including labels can be seen in the appendix. The model was build using the computer program `Inventor`. For this set-up to work, a dichroic mirror is required. These mirrors have the property that they have a certain cutoff wavelength up to which they reflect incident light and allow all light with a greater wavelength to pass through. One of these dichroic mirrors is already used in the set-up, with a cut-off wavelength of above 798 nm. For the fourth laser, a dichroic mirror must allow light with a wavelength of above 795 nm to pass and light with this or a smaller wavelength to be reflected. Additionally, each locked beam needs a PBS to differentiate between the incident beam and the one reflected on the cavity (sec. 2.3). The light that comes back from the cavity is reflected into the photodiode seen in figure 2.5.

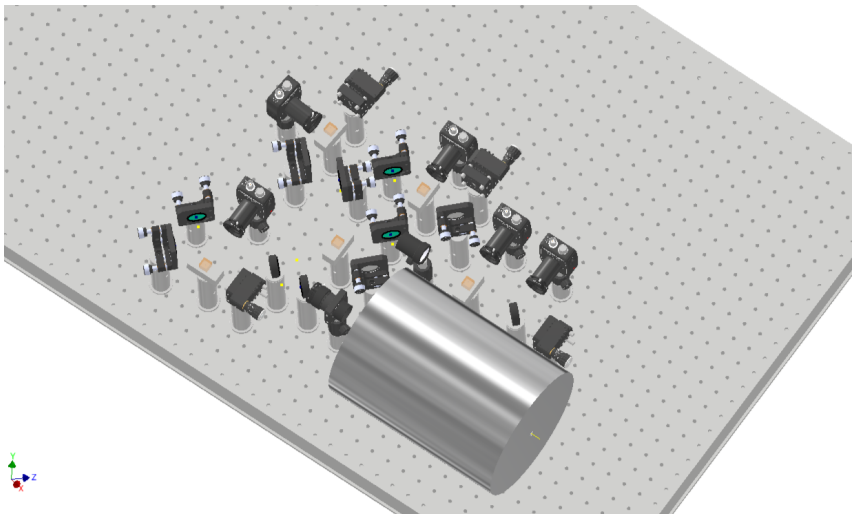

Figure 3.6: 3D model of the planned set-up of optical components in front of the ULE

3.3 Blue laser beam

3.3.1 Set-up of the optical components

The set-up of optical components used to modify the blue beam can be seen in fig. 3.7. Again, at first, a $\lambda/2$-wave plate is used to regulate the incident beam power. This time, the PBS damps the vertically polarized components of the beam into a beam dump while the rest gets transmitted. The beam diameter shortly after the output of the laser measures 1.35 mm. To narrow it down to a diameter of 500 µm, a telescope is build into the beam after the PBS. Because the AOM, that follows the telescope in the set-up of the optics, has a preferred direction of polarization of the incident photons, another $\lambda/2$-wave plate is build into the beam, which is placed before the telescope. To save space, the telescope consists of a convex and a concave lens leading to a collimated beam after the second, concave lens, that goes into the AOM. The characterization of the AOM will follow in sec. 3.3.2. The remaining optics after the AOM, which were used until coupling the beam into the fiber, are very similar to those from the infrared beam after the telescope, see fig. 3.7. The power of the beam as it comes out of the laser was (1.128 ± 0.001) W, right after the first $\lambda/2$-wave plate it was (1.050 ± 0.002) W and after the PBS only (33.63 ± 0.02) mW. Since the intensity of the beam depends very much on how the first lambda half plate is set, the last two measured values serve only to give the reader an idea of the magnitude of the intensities and losses that arise with this arrangement of optical components.

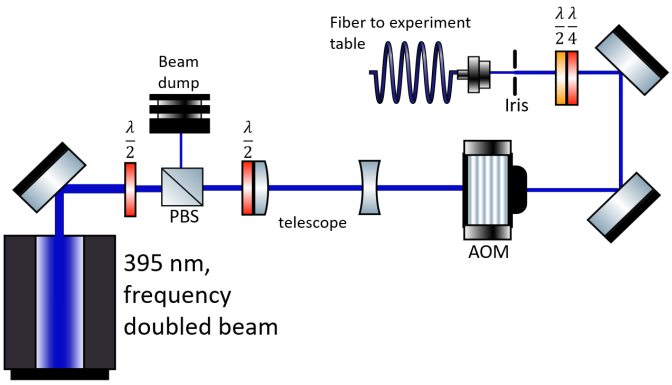

Figure 3.7: Symbolic set-up of the used optical components in the blue beam

3.3.2 Acousto-optical modulator in the blue beam

The AOM used for the blue beam is a model from *Gooch & Housego*[10]. It uses a crystal quartz as interaction material and has an active aperture of 2 mm [35].
The center frequency of this AOM is at 110 MHz. With the given active aperture, it would mean that the beam diameter of 1.35 mm[11] as it comes out of the laser would be small enough to pass the active aperture and be diffracted in it. But since the rise time of the AOM is dependent on the beam diameter, the telescope was implemented to decrease the beam diameter and thus the rise time. After the telescope, the beam had an estimated diameter of 440 µm. This value was generated by the computer program `Gaussian beam`, see fig. A.5 in the appendix. The rise time of the AOM was measured using the same set-up and the same photodiode as before. The plot of the oscilloscope data resulted in a rise time of 52.0 ns, which is close to the manufacturer's specified value of 113 ns/mm [36]. The deviation between the theoretically expected value of 49.7 ns and the result of the plot is most likely due to the fact that the beam in reality deviates from the calculated 440 µm, i.e. the beam diamter inside the crystal of the AOM is rather a little smaller than 440 µm. The result of the rise time measurement is shown in figure 3.8. Also, the diffraction efficiency of the AOM was measured. According to the manufacturer, over 99% of the incident light is transmitted [30]. This was confirmed by measuring 33.1 mW before and 32.9 mW after the AOM. Here, the diffraction efficiency into the -1^{st} order is about 56%, see fig. 3.9. The diffraction efficiency for this AOM was measured and calculated in the exact same way as it was done for the infrared AOM, see sec. 3.2.2.

[10] Model number: I-M110-2C10B6-3-GH26
[11] no error on this measurement was given by the software `Beam View - USB`

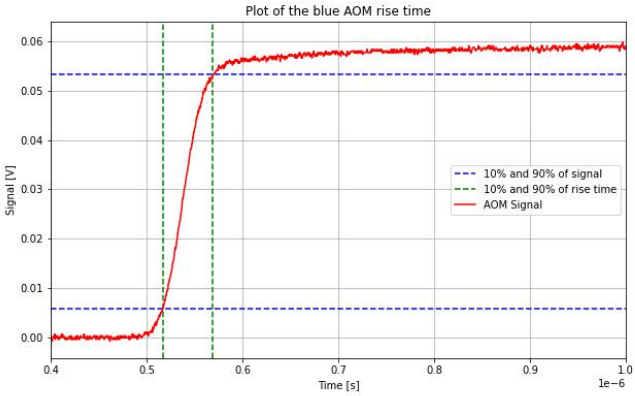

Figure 3.8: Rise time plot of the AOM in the blue beam

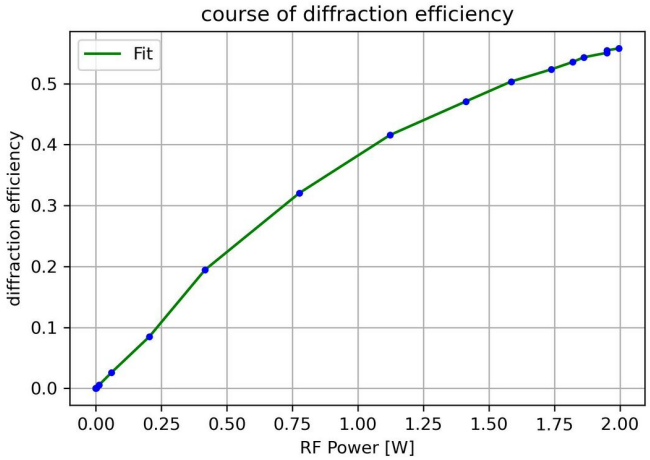

Figure 3.9: Diffraction efficiency of the AOM in the blue beam

CHAPTER 4

Outlook

In the following chapter of this work, the remaining work that still has to be done to complete the set-up of electrical components needed for PDH method. Since the frequency stabilization of the laser using PDH has not been carried out yet, this will not be part of this chapter. However, the targeted intermediate and Rydberg states of the trapped Ytterbium atoms and where in the experiment the atoms are located, when the blue laser irradiates them, will be discussed. The focus will be on the remaining components that need to be set-up as well as a theoretical description of the atomic transitions of Ytterbium rather than diving deep into the practical specifics of it.
Since this laser is already the fourth laser that is locked to the ULE cavity of this experiment, the electronic components such as the *FALC* and the *PDD-110* are already present in the experiment, whereas the *Windfreak*-Box is already built but still needs to be connected to the experiment. Also, the RF-generator *SynthUSB II* must be programmed correctly so that it supplies the mixer inside the *Windfreak*-Box with the correct frequency signal. Then, all components have to be connected according to the diagram in fig. 2.5.
The part that eventually feeds the laser with a feedback signal according to the observed deviation of the laser frequency from the reference frequency is the *FALC*. It takes the error signal and generates a control signal which adjusts the laser frequency via actuators, typically the laser diode current and a piezo transducer which affects the laser cavity length. The control signal effectively adjusts the laser frequency to reduce the error signal towards zero. This closed feedback loop suppresses fluctuations and keeps the laser tuned to the frequency required for experimentation [12].
Because the blue laser output is directly linked to the frequency of the infrared laser, see 3.1, the frequency stabilization of the infrared laser leads to a frequency stabilized blue laser. The blue laser, in turn, is used to excite the atoms trapped in a dipole trap in the main experiment (for more information on dipole traps, see [37]. One possible transition, as seen in fig 4.1,

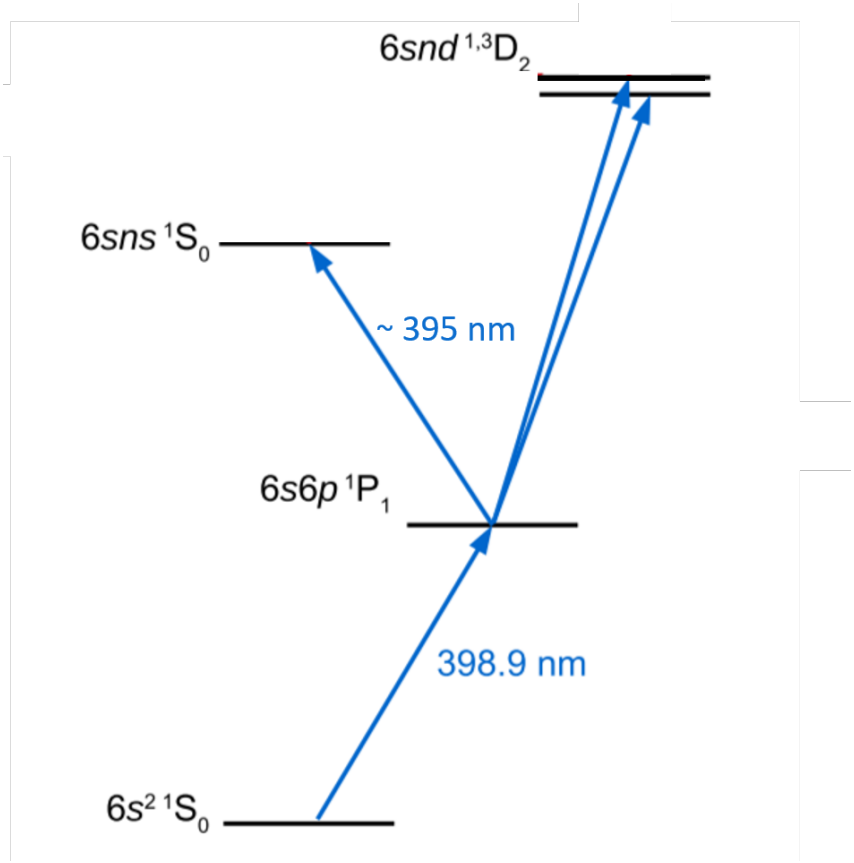

Figure 4.1: Targeted energy transition of Yb^{174} [39]

to excite the Ytterbium atoms to the Rydberg state is from the ground state $6s^2\ ^1S_0$ into the intermediate state $6s6p\ ^1P_1$ to finally the Rydberg state 6sns $^1S_0$ or 6snd $^{1,3}D_2$. With n being the principal quantum number and $n \gg 1$ in Rydbger atoms, e.g. in the order of $n = 20$ and far beyond [38]. To achieve this, the ground state is coupled with a weak, single photon laser at 399 nm to the intermediate state. This state is then excited to the Rydberg state by a strong control laser, namely the blue laser with 395 nm described in this work.

CHAPTER 5

Summary

This thesis intended to highlight the efforts involved in setting up the laser system, serving as a foundation for frequency stabilization and the excitation of Ytterbium atoms into Rydberg states.

After discussing the theoretical knowledge in section 2 necessary to understand the experimental setup, the operational mode of the laser was presented, see sec. 3.1. There, the creation of the infrared output beam was explained as well as the procedure of creating the blue laser beam.
This part was followed by section 3.2 which introduced the set-up of the optical components, that modify the infrared beam in order to carry out frequency stabilization using the PDH method. To measure the frequency of the infrared beam a wavemeter was used and measured (379.7407 ± 0.0006) THz which equals a wavelength of (789.466 ± 0.001) nm. Section 3.2.2 then describes the implementation of the acousto-optical-modulator (AOM), how it works as well as measurements that were done to characterize the modulator. These showed that the used AOM diffracts 47% of the incident beam into the -1^{st}-order and has a rise time of 58.8 ns. Possible reasons for the deviation in the double-digit nanosecond range from the value given by the manufacturer were discussed. 31% of the beam intensity of one milliwatt, measured in the -1 order, was coupled into the fiber, which is sufficient power to lock the signal to the ULE cavity. After this, electro-optical modulators were detailed, their important part in the PDH method outlined and the temperature stabilization was visually presented. Also important for the EOM, but especially the PDH procedure, are the RF-generators *SynthUSB II*, detailed in section 3.2.4. How these are integrated into the system and how they function was explained. The section about the infrared laser closed by briefly outlining a possible experimental set-up of optical components in front of the ULE cavity. Briefly because the optical components for coupling the infrared beam into the ULE cavity have so

far only been planned but not yet built.

This section was followed by a description of the set-up of optics in the blue beam. With the chosen setting of the first $\lambda/2$-wave plate and the following PBS, the beam intensity was reduced to 3% of the initial beam intensity of the laser output of 1.128 W. An AOM diffraction efficiency of 56% was reached here and a rise time of 52.0 ns was measured, which resonates with the value given by the manufacturer.

Lastly, an outlook in order to finish setting up the frequency stabilization set-up was given. One of the targeted energy transitions in the Ytterbium energy scheme was depicted, and the necessity of frequency stabilization for this experiment was underscored by the line width of a specific example.

APPENDIX A

Appendix

Figure A.1: course of the blue beam simulated using the „`Gaussian Beam`“ program

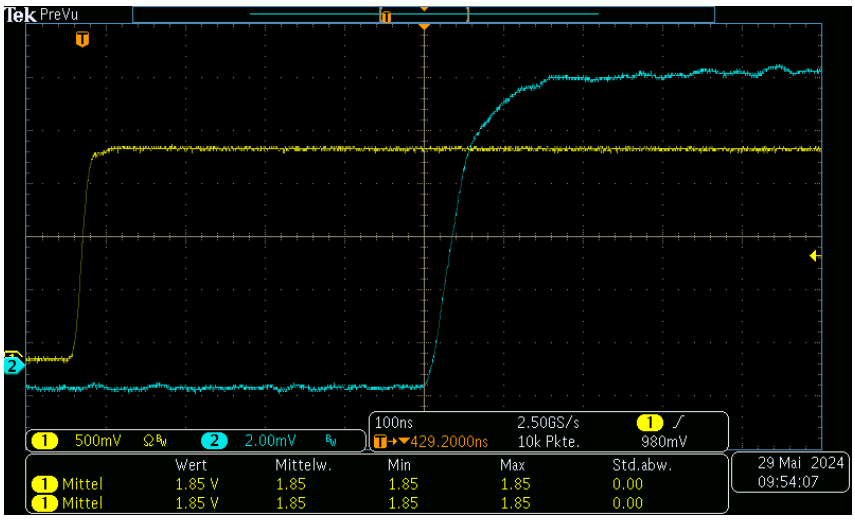

Figure A.2: Comparison of the input signal of the AOM (yellow) and the signal of the Photodiode (blue)

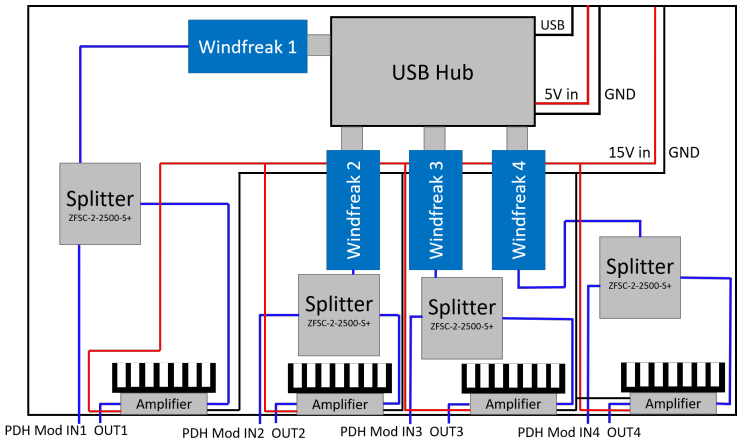

Figure A.3: Internal set-up of the housing that contains the RF-signal generator *SynthUSB II*, called „Windfreak“ in the figure, and the used electronics in each channel, incl. heatsinks, black, on each amplifier, to create the modulation frequency that is send to the EOM

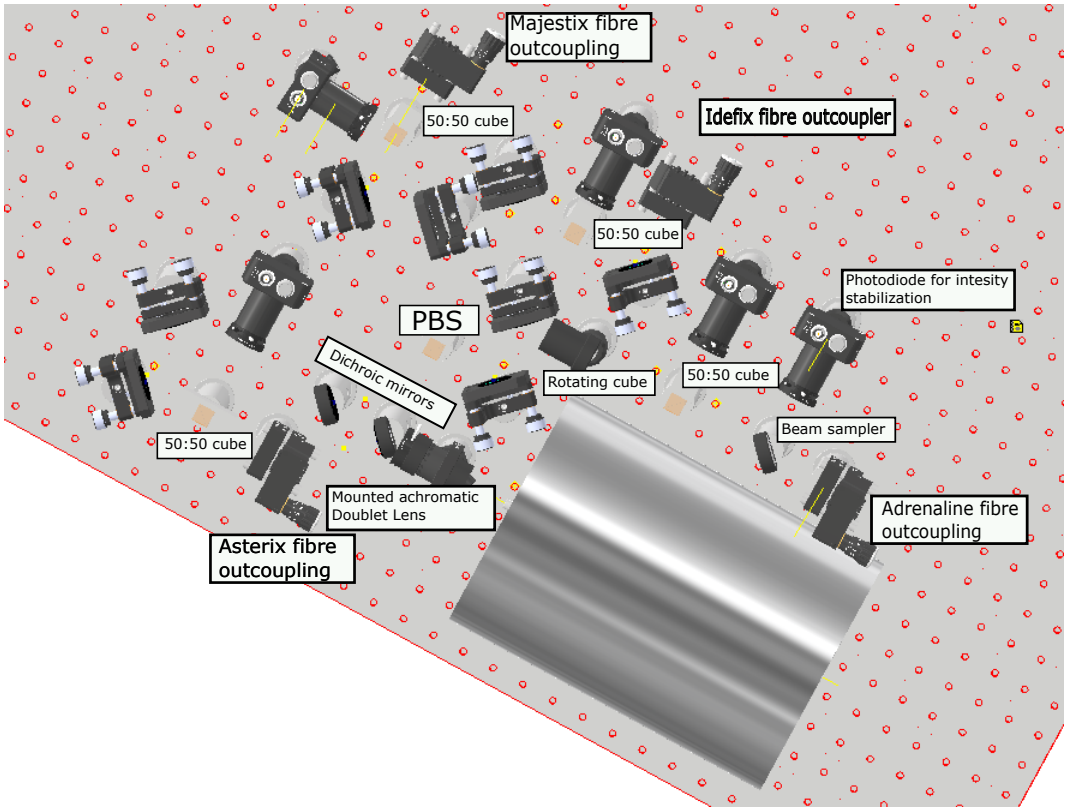

Figure A.4: 3D model of the possible set-up of optical components in front of the ULE cavity

Figure A.5: course of the blue beam simulated using the „`Gaussian Beam`“ program

Bibliography

[1] C. H. Townes, *The first laser*, A century of nature: Twenty-One Discoveries that changed science and the world chapter 8 (2003) (cit. on pp. 1, 3).

[2] O. Svelto, *Principles of Lasers*, 5th Edition, Springer, 2010, ISBN: 978-1-4419-1301-2 (cit. on pp. 1, 4, 7–9).

[3] W. Demtröder, *Experimentalphysik 3 - Atome, Moleküle und Festkörper*, 5th, Springer, 2016, ISBN: 978-3-662-49093-8 (cit. on p. 1).

[4] X. O. Z. Zhou and Y. Fang, *Prospects and applications of on-chip lasers*, eLight 3, 1 (2023) (cit. on p. 1).

[5] R. de Vivie Riedle and U. Troppmann, *Femtosecond Laser for Quantum Information Technology*, Chem. Rev. 2007,107, 5082-5100 (2007) (cit. on p. 1).

[6] O. F. C. A. und S. Hofferberth, *Nonlinear quantum optics mediated by Rydberg interactions*, J. Phys. B: At. Mol. Opt. Phys. 49 152003 (2016) (cit. on p. 1).

[7] M. D. L. et al., *Dipole Blockade and Quantum Information Processing in Mesoscopic Atomic Ensembles*, Phys. Rev. Lett. 87 (2001) (cit. on p. 2).

[8] F. u. H. Gorniaczyk, *Single-Photon Transistor Mediated by Interstate Rydberg Interactions*, Phys. Rev. Lett. 113 2014 (2014) (cit. on p. 2).

[9] *Line width of the TA-SHG pro*, https://www.toptica.com/products/tunable-diode-lasers/frequency-converted-lasers/ta-shg-pro, last call: 02.07.2024 (cit. on p. 2).

[10] C. Maier, *Laser system for the Rydberg excitation of Strontium ions*, University of Innsbruck (2013) (cit. on p. 2).

[11] A. L. W. Zinth and W. Kaiser,
The long journey to the laser and its rapid development after 1960,
Eur. Phys. J. H 36, 153–181 (2011) (cit. on p. 3).

[12] Moglabs, *Pound-Drever-Hall Locking with the FSC, AN002*,
https://www.moglabs.com/support/appnotes (cit. on pp. 3, 26).

[13] W. Demtröder, *Laserspektroskopie 1, chapter 5*, 6th Edition, Springer, 2011
S. 161 ff, 180 (cit. on pp. 4, 8, 10).

[14] R. D. M. Bitarafan, *On-Chip High-Finesse Fabry-Perot Microcavities for Optical Sensing and Quantum Information*, Sensors 2017, 17(8), 1748 (2017) (cit. on p. 5).

[15] E. Black, *An introduction to Pound–Drever–Hall laser frequency stabilization*,
Am. J. Phys. 69, 79–87 (2000) (cit. on pp. 5, 6, 11, 12).

[16] D. Meschede, *Optik, Licht und Laser*, 3th, Vieweg und Teubner, 2008,
ISBN: 978-3-8348-9288-1 (cit. on p. 5).

[17] *Diode laser*, https://www.chemie.de/lexikon/Laserdiode,
last call: 06.06.2024 (cit. on p. 8).

[18] A. M. E.N. Myasnikov,
Band theory of semiconductors and autolocalization of electrons,
Physics Letters A 286 210–216 (2001) (cit. on p. 8).

[19] K. W. C. Hawthorn and R. Scholten, *Littrow configuration tunable external cavity diode laser with fixed direction output beam*,
School of Physics, The University of Melbourne (2001) (cit. on p. 9).

[20] *High-power, tunable, frequency-doubled diode laser*,
https://www.toptica.com/products/tunable-diode-lasers/frequency-converted-lasers/ta-shg-pro, last call: 17.06.24 (cit. on p. 9).

[21] *Physical properties of Gaussian beams*, http://www.optique-ingenieur.org/en/courses/OPI_ang_M01_C03/co/Contenu_08.html,
last call: 28.06.2024 (cit. on p. 10).

[22] ". Pampaloni and J. Enderlein",
Gaussian, Hermite-Gaussian, and Laguerre-Gaussian beams: A primer,
Am. J. Phys, arXiv preprint physics/0410021 (2004) (cit. on p. 10).

[23] E. Fitch, *The spectrum of modulated pulses*, Journal of the IEE - Part IIIA: Radiocommunication Vol 94, Iss 13, Mar Apr 1947, p. 556 – 564 (1947)
(cit. on p. 12).

[24] *Used Cavity in the YQO experiment*, https://wiki.nqo.uni-bonn.de/index.php/YQO:Stable_Lasers_reference_cavity, last call: 21.06.2024 (cit. on p. 14).

[25] A. H. "P. Franken and G. Weinreich", *Generation of Optical Harmonics*, Phys. Rev. Lett. 7, 118 (1961) (cit. on p. 16).

[26] *SHG pro, Frequency doubling unit*, https://www.toptica.com/products/tunable-diode-lasers/frequency-converted-lasers/shg-pro, last call: 20.06.2024 (cit. on p. 16).

[27] *SHG pro gallery*, https://www.toptica.com/products/tunable-diode-lasers/frequency-converted-lasers/shg-pro, last call: 20.06.2024 (cit. on p. 16).

[28] *Definition optical density*, https://www.thorlabs.com/newgrouppage9.cfm?objectgroup_id=266&pn=NE20A, last call: 01.07.2024 (cit. on p. 17).

[29] I. Chang, *Acousto-optic devices and applications*, Handbook of optics **2** (1995) 12 (cit. on p. 18).

[30] M. H. e. a. M Aldous J. Woods, *Carrier frequency modulation of an acousto-optic modulator for laser stabilization*, Opt. Express 25, 12830-12838 (2017) (cit. on pp. 18, 24).

[31] R. Paschota, *optical modulators based on the acousto-optic effect*, https://www.rp-photonics.com/acousto_optic_modulators.html () (cit. on p. 18).

[32] https://gandh.com/products/acousto-optics/modulators/aomo-3080-122, last call: 01.07.2024 (cit. on pp. 19, 20).

[33] T. C. G. Sinatkas and E. Kriezis, *Electro-optic modulation in integrated photonics*, J. Appl. Phys. 130 (1): 010901 (2021) (cit. on p. 21).

[34] *SynthUSBII: 34MHz – 4.4GHz USB RF Signal Generator*, https://windfreaktech.com/product/usb-rf-signal-generator/ (cit. on p. 21).

[35] *Spec sheet of G&H AOM*, https://gandh.com/products/acousto-optics/modulators/i-m110-2c10b6-3-gh26, last call: 27.06.2024 (cit. on p. 24).

[36] https://gandh.com/products/acousto-optics/modulators/i-m110-2c10b6-3-gh26, last call: 01.07.2024 (cit. on p. 24).

[37] A. Harsono, *Dipole trapping and manipulation of ultra-cold atoms*, Oxford University (2006) (cit. on p. 26).

[38] T. F. Gallagher, *Rydberg atoms*, Rep. Prog. Phys. 51 143 (1988) (cit. on p. 27).

[39] W. M. H. Lehec A. Zuliani and E. L.-K. et al., *Laser and microwave spectroscopy of even-parity Rydberg states of neutral ytterbium and multichannel-quantum-defect-theory analysis*, Phys. Rev. A 98, 062506 (2018) (cit. on p. 27).

List of Figures